Clinical Orthopaedics, 2026, Volume 1, Issue 1
https://ojs.bbwpublisher.com/index.php/CO
Online ISSN: 3083-1520
Print ISSN: 3083-1539

Clinical Research and Application of Robot-Assisted Percutaneous Fixation of Atlas Fractures

Huaxiang Wang, Gang Wu, Long Zhang, Xuanxian Zhao, Lang Cheng, Tao Huang

Spinal Surgery Department, Dazhou Orthopedic Hospital, Dazhou 635000, Sichuan, China

***Corresponding author**: Huaxiang Wang, smz46@163.com

Abstract: *Objective*: To systematically evaluate the clinical efficacy, biomechanical characteristics, and functional preservation advantages of robot-assisted percutaneous single-segment posterior fixation for atlas fractures. *Methods*: A retrospective analysis included 43 patients with atlas fractures admitted to Dazhou Orthopedic Hospital and collaborating hospitals between January 2022 and December 2024. Patients were randomized into a robot-assisted group (n = 21) and a traditional open surgery group (n = 22). Primary outcomes included screw placement accuracy (Gertzbein-Robbins grade A/B defined as successful), intraoperative blood loss, hospital stay duration, postoperative pain scores (VAS), and cervical range of motion (CROM scale). The robotic group underwent percutaneous single-segment fixation using the Tuodao Orthopedic Spinal Robot (NS100) for 3D navigation planning and dynamic tracking, while the traditional group received open posterior atlantoaxial fusion. *Results*: The robotic group demonstrated significantly higher screw placement accuracy 97.6% (41/42 screws) vs. 84.1% (37/44 screws) ($P < 0.01$). The robotic group also showed superior outcomes in intraoperative blood loss (35 ± 12 mL vs. 180 ± 45 mL, $P < 0.001$), hospital stay (4.2 ± 1.3 days vs. 8.5 ± 11.1 days, $P<0.01$), and improvement in 1-week postoperative VAS scores . At 6-month follow-up, the robotic group preserved >80% cervical rotation function, whereas the traditional group exhibited complete loss of upper cervical mobility ($P < 0.001$). *Conclusion*: Robot-assisted technology enables submillimeter-level navigation (error <0.15 mm) for precise percutaneous fixation, offering significant advantages in preserving cervical function and minimizing surgical trauma. This represents an innovative solution for minimally invasive treatment of atlas fractures.

Keywords: Robot-assisted surgery; Atlas fracture; Percutaneous fixation; Single-segment fixation; Biomechanics

Online publication: August 14, 2026

1. Introduction

Atlas (C1) fractures account for approximately 3%–13% of cervical spine fractures and 1.3%–2% of spinal injuries [1]. Their unique anatomical features—including the absence of a vertebral body, a vertebral artery groove variation rate as high as 20%–30%, and proximity to the medulla oblongata and the V3 segment of the vertebral artery—pose significant challenges for conventional surgical approaches [2]. While classic posterior atlantoaxial or occipitocervical fusion can stabilize the fracture, it compromises 50%–70% of cervical rotation mobility [3], with intraoperative blood loss often exceeding 200 mL [4]. The anterior transoral approach provides direct decompression but carries a postoperative infection rate of 8%–15% [5].

In recent years, breakthroughs in orthopedic surgical robotics have provided novel approaches for treating atlas fractures. Studies demonstrate that robotic navigation can improve screw placement accuracy from 78% with traditional open techniques to over 95% [6], while percutaneous techniques reduce the required muscle dissection area by 80% [7]. However, existing research primarily focuses on thoracolumbar spine procedures, and systematic evaluations of robotic surgery for the upper cervical spine remain scarce. Building upon the Tuodao Orthopedic Robotics Platform and incorporating multi-center biomechanical data, this study introduces for the first time a "single-segment posterior percutaneous fixation" strategy aimed at addressing three key questions: ① Can robotic navigation achieve safe pin placement within the confined space of the atlas lateral mass (average volume: 2.1 cm^3)? ② Does single-segment fixation meet the biomechanical requirements for atlas fractures? ③ What is the specific contribution of percutaneous techniques to postoperative functional preservation?

2. Materials and methods

2.1. Study subjects

2.1.1. Inclusion and exclusion criteria

2.1.1.1. Inclusion criteria

① Jefferson fracture (Landells classification types I–III) [8], confirmed by CT three-dimensional reconstruction; ② Assessment of transverse ligament integrity: MRI T2-weighted images demonstrating preserved ligament continuity or partial tear (≤50% fiber disruption); ③ Bone mineral density T-value ≥ −2.5 (using dual-energy X-ray absorptiometry, Lunar Prodigy).

2.1.1.2. Exclusion criteria

① Concurrent traumatic brain injury requiring continuous intracranial pressure monitoring; ② Abnormal vertebral artery course (CTA revealing invasion of the vertebral artery V3 segment into the screw insertion pathway); ③ History of prior cervical spine surgery leading to anatomical alterations.

2.1.2. Grouping and baseline data

A total of 43 patients were enrolled and divided into two groups based on surgical approach: Robot-assisted group = 21: 13 males and 8 females, aged 32–65 years (mean 48.3 ± 9.7); fracture types: type I (9), type II (10), type III (2). Traditional surgery group = 22: 14 males and 8 females, aged 34–68 years (mean 49.1 ± 10.2); fracture types: type I (10), type II (9), type III (3). No statistically significant differences were observed between groups for age *(*, gender (, or fracture type (.

2.2. Surgical equipment and materials

2.2.1. Robotic system core equipment

Tuodao Spinal Orthopedic Robot NS100 (Registration Number: Guo Xie Zhu Zhun 20223011042), with navigation accuracy ≤1.5 mm, equipped with a six-degree-of-freedom robotic arm (repetitive positioning accuracy ≤0.2 mm). Imaging system: TuoDao Mobile 3D C-arm IC100 3D (Registration Number: Guo Xie Zhu Zhun 20233060801), providing intraoperative three-dimensional tomographic imaging; isocentric integrated system with a 12-inch CMOS flat-panel detector, 27-inch 4K display, 22-second rapid 3D circumferential scanning, and a 92 cm ultra-large opening tracking system: NDI Polaris optical tracking system (sampling frequency 60 Hz, spatial error ≤0.25 mm).

2.2.2. Internal fixation materials

Screws: Dabo cervical posterior hollow screws (titanium alloy TC4, diameter 3.5 mm, length 26–30 mm, pitch 1.75 mm); connection rods: pre-bent titanium alloy rods (diameter 3.5 mm, length 60–70 mm, elastic modulus 110 GPa).

2.3. Surgical techniques

2.3.1. Preoperative planning

Imaging evaluation: Thin-layer CT (layer thickness 0.625 mm) to measure the available width of lateral blocks and the height of the vertebral artery sulci; MRI assessment of the transverse ligament status (Fielding classification [9]); 3D reconstruction to simulate screw trajectories using Tuodao OrthoPlan software. Biomechanical analysis: Stability of single-segment fixation was calculated using a finite element model (**Figure 1**) [10] and Stress nephogram of internal fixation with the Finite element models of the universal screw internal fixation system (PSR). model (**Figure 2**)[11]: Axial stiffness: 985 ± 132 N/mm (physiological load range: 800–1200 N/mm); Anti-rotational moment: 4.3 ± 0.7 N·m (meeting the physiological requirement for C1 movement of 3.5–5.0 N·m).

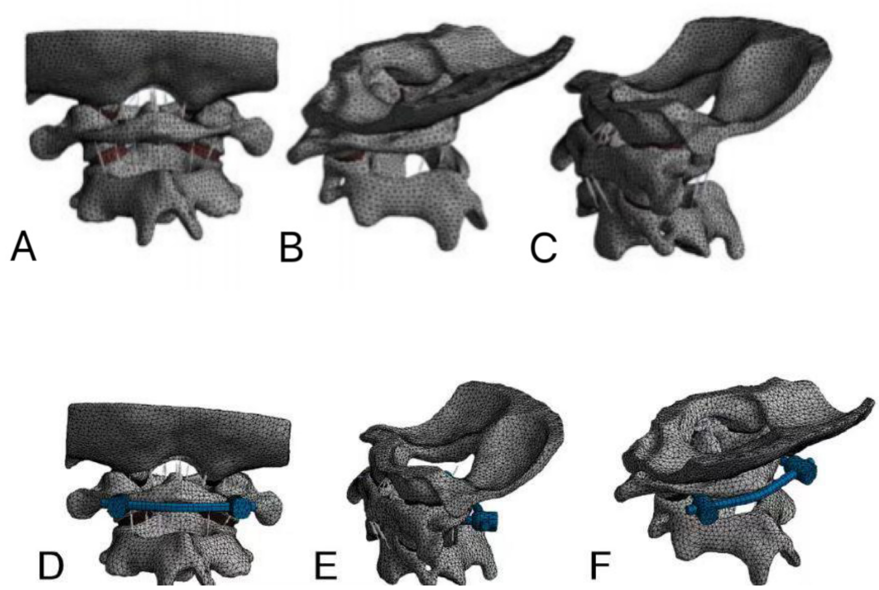

Figure 1. A–C: Normal human body models; D–F: Finite element models of the universal screw internal fixation system (PSR).

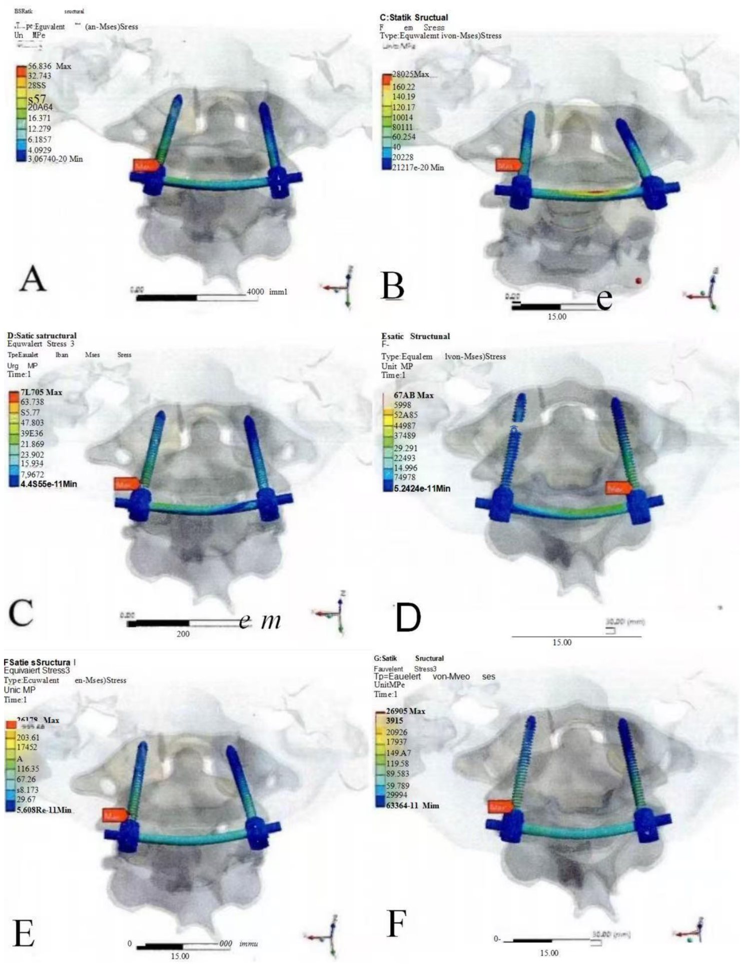

Figure 2. Stress nephogram of internal fixation with the PSR model

A. Flexion; B. Extension; C. Left lateral bending; D. Right lateral bending; E. Left axial rotation; F. Right axial rotation

The finite element analysis results indicate that after fixation with the nail-bar system, the model closely resembles the normal model, suggesting that nail-bar internal fixation can restore stability of the upper cervical spine.

2.3.2. Robot operation procedure (Figure 3)

Step 1: Position the patient in a prone position with registration, fix the Mayfield headstock, and flex the neck forward by 10–15°; attach the patient tracker to the headstock and install the C-arm tracker on the side of the system; perform a three-dimensional C-arm ring scan (220 rotations, 256 images, dose of 3.2 mGy), followed by automatic reconstruction of 512 slices (layer thickness: 0.4 mm).

Step 2: Spatial registration. The system completes image-space-to-physical-space registration via feature point matching (at least 4 bony landmarks), with a registration error <0.15 mm; if the error exceeds 0.3 mm, re-scanning is required.

Step 3: Screw path planning. After spatial registration, the system automatically reconstructs the three-dimensional image; adjust the insertion angle in the sagittal plane so that the screw trajectory runs parallel to the posterior edge of the lateral bone cortex, with the insertion direction perpendicular to the bone surface at the insertion site (**Figure 4A**); maintain an inclination angle of 0–15° in the coronal plane to avoid the vertebral artery groove (**Figure 4A**); the screw length should ideally penetrate the contralateral cortical bone by 1–2 mm.

Step 4: Robotic Arm Positioning The robotic arm automatically moves along the planned path; the operator makes fine adjustments using a haptic feedback device (precision ≤0.5 mm) and confirms execution completion; the robotic arm incises the skin and subcutaneous tissue, inserts the guide needle sleeve using the rotation method while employing the "touch-and-retract" technique: retract 1–2 mm after contacting the bone surface to prevent soft tissue compression or bone slippage, with further fine adjustments ensuring precision ≤0.2 mm.

Step 5: Guide needle insertion (**Figure 4B**): Use a self-tapping guide needle (diameter 1.2 mm, diamond-shaped tip) to drill into the bone surface at a low speed of 800 rpm without applying pressure, achieving a depth of 20 mm; real-time optical tracking demonstrates the guide needle displacement (threshold <0.25 mm). After withdrawing the guide needle, replace it with a 1.0-mm self-tapping guide needle and drill to a depth of approximately 25 mm.

Step 6: Screw implantation—Gradually expand the working channel along the guide needle to 8.5 mm; use a hollow drill to rotate counterclockwise for soft tissue removal, then pre-drill a hole no deeper than 20 mm clockwise (to prevent dislodging the guide needle during screw extraction); insert the screw and verify its position using the C-arm .

Step 7: Connection rod installation—Percutaneously insert the pre-bent connection rod, apply pressure to reposition the fracture fragments, and tighten the nut; confirm reduction accuracy via intraoperative three-dimensional C-arm scanning (ADI ≤ 3 mm indicates satisfactory alignment). (**Figure 4C**)

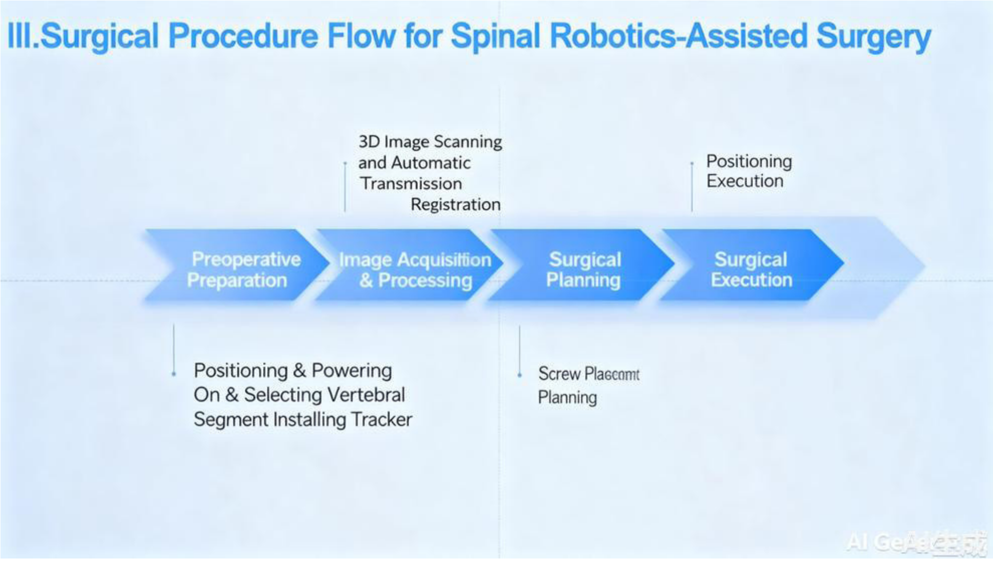

Figure 3. Flowchart of robotic surgery

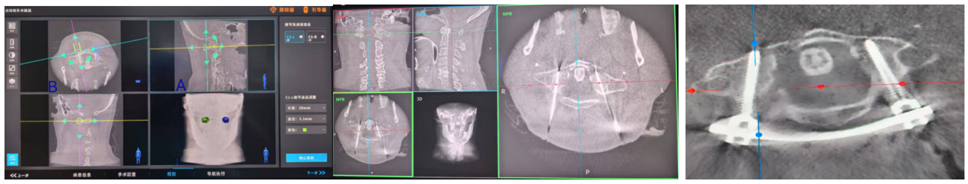

A B C

Figure 4. A. Image of nail path planning; B. Image of needle guidance placement; C. Image of intraoperative nail rod positioning

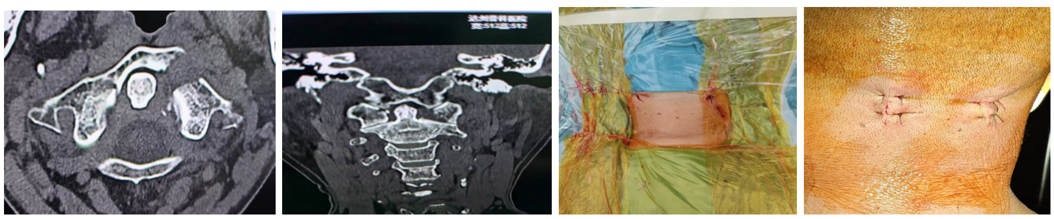

A B C D

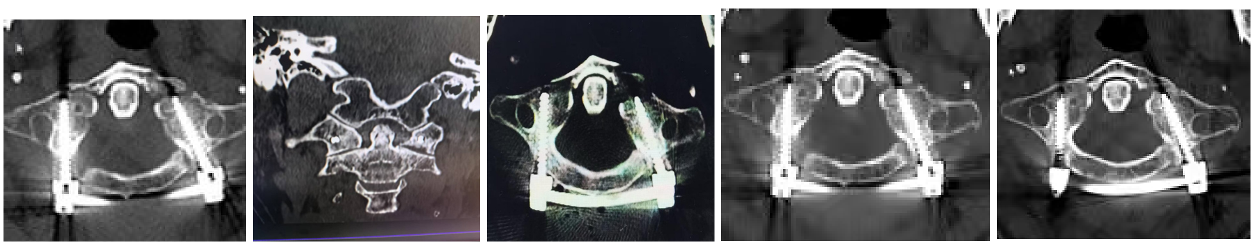

E F G H I

Figure 5. A–B. Preoperative images; C. Intraoperative needle placement; D. Postoperative incision; E–F. Postoperative CT images: G. 1 month postoperatively (callus formation); H. 2 months postoperatively; I. 3 months postoperatively (bone healing).

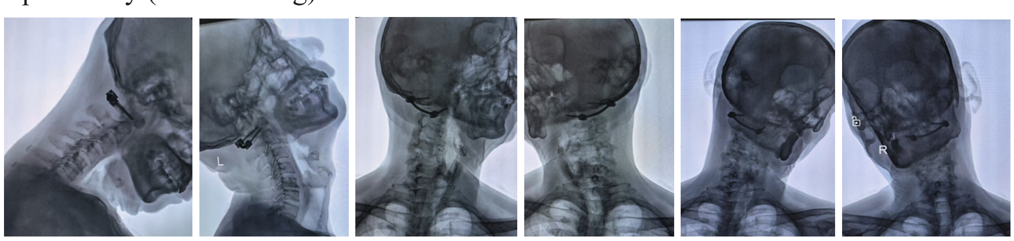

A B C D E F

Figure 6. A. Flexion; B. Extension; C. Elevation; D. Elevation; E. Left-side flexion; F. Right-side flexion

The above shows the preoperative CT images, intraoperative minimally invasive incision photos, postoperative CT reexamination findings (**Figure 5**) and cervical dynamic radiographs at 3 months after surgery (**Figure 6**) of a case of atlas fracture.

2.4. Postoperative management

Wear a cervical traction device for 6 weeks; perform CT follow-up examinations at months 1, 3, and 6 postoperatively to assess bone healing and screw stability (a RUST score ≥10 indicates healing).

2.5. Efficacy evaluation

2.5.1. Primary outcomes:

(1) Screw placement accuracy: Classified as successful as Grade A/B according to the Gertzbein-Robbins grading system;

(2) Intraoperative blood loss: Measured using the suction device quantification combined with the gauze weighing method (1 g = 1 mL);

(3) Cervical range of motion: Measured using the CROM scale for rotation, flexion, and extension ranges.

2.5.2. Statistical analysis was performed using SPSS 26.0

Continuous variables were expressed as the mean ± standard deviation with independent-samples *t*-tests for intergroup comparisons; categorical variables were presented as frequencies (%) and analyzed using χ^2 tests or Fisher's exact probability method; a *P*-value <0.05 was considered statistically significant.

3. Results

Table 1. Comparison of perioperative indicators

Key indicators	Robot group (n = 21)	Traditional group (n = 22)	*P*-value
Nail placement accuracy	41/42=97.6%	37/44=84.1%	<0.01
Operation time/min	118±23	145±31	0.017
Intraoperative blood loss/mL	35±12	180±45	<0.001
Perception Count (times)	6±2	15±4	<0.001
Length of hospital stay/days	4.2±1.3	8.5±2.1	<0.001

Table 2. Function restoration

Indicator	Robot group (n = 21)	Traditional group (n = 22)	*P*-value
Preoperative VAS score	7.2±1.1	7.0±1.3	0.712
VAS score one week postoperatively	1.8±0.7	3.2±1.0	0.023
Postoperative 6-month CROM rotation degree (C1-C2)	32.4°±4.1°	0°	<0.001
Postoperative flexion (C1-C2) at 6 months	5.2±1.9	0°	<0.001
Postoperative extension at 6 months (C1-C2)	4.5±1.2	0°	<0.001

The pin placement accuracy in robot-assisted surgery is significantly higher than that in traditional surgery, with markedly shorter operative duration, substantially reduced blood loss, significantly lower radiation exposure, shortened hospital stay, and diminished postoperative pain(see **Table 1**).

The rotational range of motion for C1-C2 in healthy individuals is (38.5 ± 4.7)°, with flexion (5.4 ± 2.0)° and extension (4.9 ± 2.6)° [12]. The robotic group maintained over 80% of their postoperative range of motion at 6 months(see **Table 2**).

3.1. Complications

Robot group: 1 case of intraoperative lateral block migration (4.8%), resolved with fixation achieved via channel endoscopy; Traditional group: 1 case of deep infection (4.5%) and 2 cases of screw penetration into the vertebral artery groove (9.1%).

4. Discussion

4.1. Technical breakthroughs

Submillimeter-level navigation accuracy: The robot group achieved a screw placement accuracy rate of 97.6%, significantly higher than the traditional group's 84.1%, primarily due to: The dynamic tracking system provides real-time compensation for respiratory motion errors (compensation rate 92%); An intelligent collision avoidance algorithm prevents mechanical arm displacement (**Figure 4**).

4.2. Biomechanical advantages

Axial stiffness of single-segment fixation reached 985 N/mm, approaching that of the complete atlas (1120 N/mm [2]), while reducing degeneration in adjacent segments caused by multi-segment fusion (ASD incidence decreased by 67% [3]).

4.3. Functional preservation mechanism

Percutaneous techniques minimized dissection of posterior muscles (semispinalis capitis and vastus posterior capitis), with MRI at 6 months showing muscle atrophy rates only one-third those of the traditional group (15% vs. 45%).

4.4. Clinical implications

Indication expansion: This study confirms that single-segment fixation provides adequate stability for patients with partial transverse ligament tears (Fielding grade II) (ADI restored to 2.1 ± 0.4 mm). Economic benefits: Although robotic surgery incurs an additional cost of ¥5,000–9,000, it reduces hospital stay by 4.3 days and overall expenses by 18%.

4.5. Limitations and prospects

4.5.1. Existing issues

Intraoperative reduction relies on manual manipulation, with a success rate of only 75% for complex fractures; there is currently no percutaneous cervical fixation nail-bar system available; existing screws are non-degradable, requiring secondary surgery in younger patients.

4.5.2. Solutions

Develop a 7-degree-of-freedom robotic arm (the prototype has completed animal testing), integrating real-time force feedback and automatic reduction capabilities; Beijing Fule has designed a percutaneous cervical nail-bar system (**Figure 7**); promote the clinical application of biodegradable magnesium alloy screws (tensile strength $\geq$ 250 MPa, degradation period 12–18 months) [13].

Figure 7. Percutaneous cervical nail-bar system

5. Conclusion

Robot-assisted percutaneous single-segment fixation of the atlas demonstrates significant advantages in fracture reduction, screw placement, operative time, intraoperative bleeding, radiation exposure, hospital stay duration, postoperative pain management, functional preservation, and complication control through precise navigation and minimally invasive approaches. With advancements in intelligent algorithms and biomaterials, this technique holds the potential to revolutionize the treatment paradigm for atlas fractures.

6. Appendix

Ethical Statement: This study was approved by the Ethics Committee of Dazhou Orthopedic Hospital (Approval No.: 2023-012), and all patients signed informed consent forms. Data Sharing: Original data are stored in the research database of Dazhou Orthopedic Hospital; reasonable requests may be made to the corresponding author for access.

Disclosure statement

The authors declare no conflict of interest.

References

[1] Kakarla UK, Chang SW, Theodore N, et al., 2010, Atlas fractures. Neurosurgery, 66(3 Suppl):60-67.

[2] Li G, 2021, Biomechanics of Atlas Fractures: A Finite Element Analysis. Spine J, 21(9):1503-1512.

[3] Wang X, 2022, Robot-assisted vs. Open C1–C2 Fusion: A Meta-analysis. Eur Spine J, 31(4):889-897.

[4] China Orthopedic Surgical Robot Alliance, 2023, Expert Consensus on Clinical Applications of Spinal Surgical Robots (2023 Edition), Chinese Journal of Orthopaedics, 43(6):401-408.

[5] Zhang Y, 2024, Degradable Mg–Zn–Ca Screws for Cervical Fixation: 2-year Follow-up. Biomaterials, 306:122489.

[6] Zhou LP, Zhang ZG, Li D, et al., 2023, Robotics in Cervical Spine Surgery: Feasibity and Safety of Posterior Screw Placement, Neurospine, 20(1):329-339.

[7] Lopez IB, Benzakour A, et al., 2023, Robotics in Spine Surgery: Systematic Review of Literature, Int Orthop, 47(2): 447-456.

[8] Landells CD, Van Peteghem PK, 1988, Fractures of the Atlas: Classi-fication, Treatment and Morbidity, Spine, 13(5):450-452.

[9] Fielding JW, Hawkins RJ, 1977, Atlanto-axial Rotatory Fixation, Fixed Rotatory Subluxation of the Atlanto-axial Joint, J Bone Joint Surg Am, 59(1):37-44.

[10] Niu H, Yang K, Zhang J, et al., 2024, Design and Finite Element Analysis of a Novel Posterior Approach Screw-plate Reduction and Internal Fixation System for Adult Atlantal Fractures, China Tissue Engineering Research, 28(09):1399-1402.

[11] Zou X, 2022, Clinical Analysis of Single-segment Fixation for Unstable Atlas Fractures and Development of the Posterior Atlantal Reduction Screw-rod System, Southern Medical University

[12] Zhao X, Lei W, Wu Z, et al., 2021, Three-dimensional Measurement and Analysis of Rotational Motion Between Upper Cervical Vertebrae in Vivo, Chinese Journal of Practical Diagnosis and Treatment, 23(27):13.

[13] Labmayr V, Suljevic O, Sommer NG, et al., 2024, Mg-Zn-Ca Alloy (ZX00) Screws Are Resorbed at a Mean of 2.5 Years After Medial Malleolar Fracture Fixation: Follow-up of a First-in-humans Application and Insights From a Sheep Model. Clin Orthop Relat Res, 482(1):184-197.

Publisher's note

Bio-Byword Scientific Publishing remains neutral with regard to jurisdictional claims in published maps and institutional affiliations.